Spectroscopy of Donor−π−Acceptor Porphyrins for Dye-Sensitized Solar Cells

Ioannis Zegkinoglou,[†,‡] Maria-Eleni Ragoussi,[§] C. D. Pemmaraju,[∥] Phillip S. Johnson,[†] David F. Pickup,[⊥,#] Jose Enrique Ortega,[⊥,#,▽] David Prendergast,[∥] Gema de la Torre,[§] and F. J. Himpsel[†,]*

[†]Department of Physics, University of Wisconsin—Madison, 1150 University Avenue, Madison, Wisconsin 53706, United States
[‡]Advanced Light Source, Lawrence Berkeley National Laboratory, Berkeley, California 94720, United States
[§]Departamento de Química Orgánica, Facultad de Ciencias, Universidad Autónoma de Madrid, Campus de Cantoblanco, 28049 Madrid, Spain
[∥]The Molecular Foundry, Lawrence Berkeley National Laboratory, Berkeley, California 94720, United States
[⊥]Centro de Física de Materiales (CSIC-UPV-EHU), Material Physics Center, 20018, San Sebastián, Spain
[#]Departamento de Física Aplicada I, Universidad del País Vasco, 20018, San Sebastián, Spain
[▽]Donostia International Physics Center, 20018, San Sebastián, Spain

S *Supporting Information*

ABSTRACT: A recent improvement in the design of dye-sensitized solar cells has been the combination of light-absorbing, electron-donating, and electron-withdrawing groups within the same sensitizer molecule. This dye architecture has proven to increase the energy conversion efficiency of the cells, leading to record efficiency values. Here we investigate a zinc(II)-porphyrin-based dye with triphenylamine donor groups and carboxyl linkers for the attachment to an oxide acceptor. The unoccupied energy levels of these three moieties

are probed selectively by element-sensitive X-ray absorption spectroscopy at the K-edges of nitrogen and carbon. These results are complemented by ultraviolet/visible spectroscopy to obtain the optical band gap and the occupied molecular levels. Density functional theory and time-dependent density functional theory are employed to obtain a detailed understanding of the X-ray and optical absorption spectra. The attachment of electron-donating groups to the porphyrin ring significantly delocalizes the highest occupied molecular orbital (HOMO) of the molecule. This leads to a spatial separation between the HOMO and the lowest unoccupied molecular orbital (LUMO), with the HOMO having significant weight in the amine donors, while the LUMO remains localized in the porphyrin ring and the acceptor group. Such spatial separation of the frontier orbitals reduces the recombination rate of photoinduced electrons and holes, thus enhancing the energy conversion efficiency.
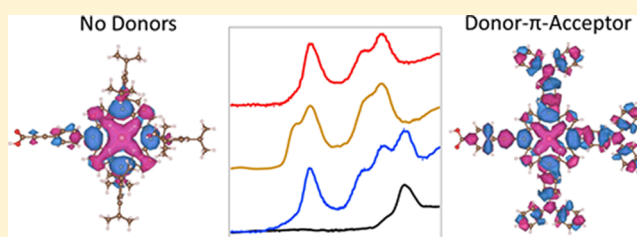
INTRODUCTION

Dye-sensitized solar cells (DSSCs) are promising alternatives to silicon-based and thin-film photovoltaic technologies for solar energy conversion.[1] The fact that they can be easily manufactured from low-cost, earth-abundant, and environmentally friendly materials makes them particularly attractive. Advances in the field have led to a significant increase of their power-conversion efficiency, reaching a record of more than 12% in recent years.[2−4] A further efficiency increase is, however, required in order to achieve grid parity with conventional fossil fuels and open the path for large-scale commercialization.

Ruthenium-based organometallic compounds adsorbed on titania (TiO$_2$) nanostructured surfaces, in combination with iodide/triiodide redox electrolytes, have traditionally been used to yield the highest efficiency rates.[5] Recently, organic dyes containing electron-rich and electron-poor sections connected via a conjugated (π) bridge have been proposed as new candidates for high-efficiency DSSCs, replacing costly sensitizers containing the rare metal ruthenium.[4,6,7] The "push−pull" architecture of these "donor−π−acceptor" (D−π−A) molecules facilitates the spatial separation of electrons and holes and thus decreases their recombination rate. Inexpensive, metal-free thiophene-based molecules with D−π−A structures have given promising results, providing efficiencies of up to 7% and high open-circuit voltages.[8−10] Even higher efficiencies have been achieved with dyes which use porphyrin macrocycles as π-bridges.[11] The most notable example is a zinc(II)-porphyrin dye containing diarylamino-groups as electron donors and ethynylbenzoic acid moieties as electron-accepting anchoring groups, which reached an efficiency of 12.3% in a prototype cell.[4]

Chart 1. Structures of the π−Acceptor Dye Molecule GT14, the Donor−π−Acceptor Molecule GT15, and of the Donor Reference Molecule tris(DPA)[a]

GT14   GT15   Tris(DPA)
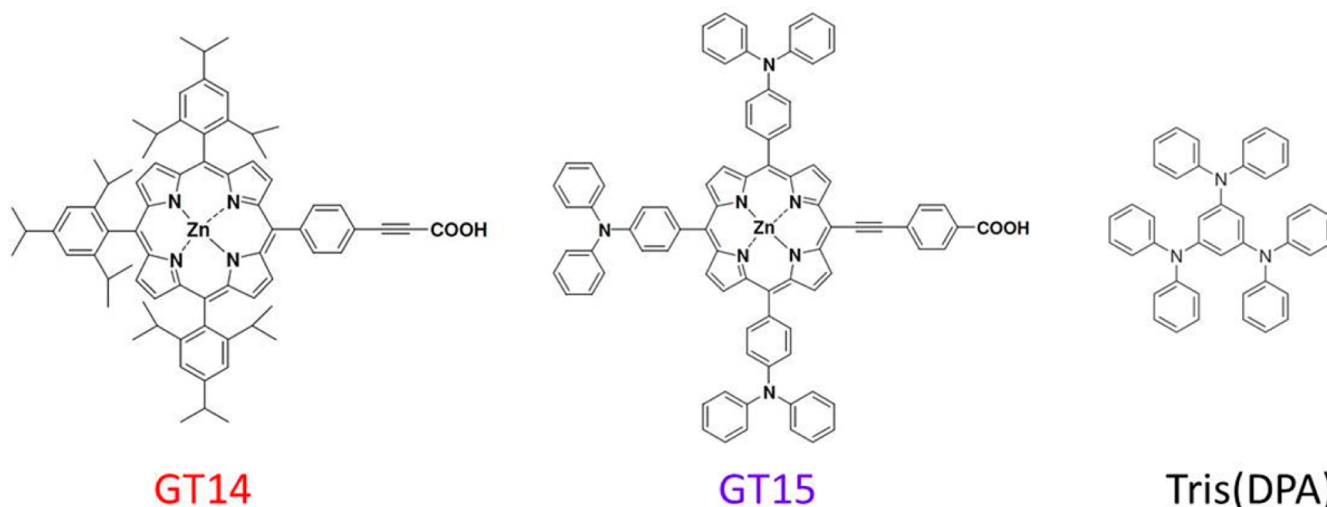
[a]The latter consists of electron-donating groups, which are similar to the triphenylamine groups which form the donors in GT15. The COOH group in GT14 and GT15 provides a link to oxide acceptors.

For the design of efficient molecular architectures, it is crucial to determine the energy levels of the three components of D−π−A sensitizers, as well as the location of the relevant orbitals within the D−π−A complex. An element-specific method is needed to probe valence energy levels at specific atoms. Near-edge X-ray absorption fine structure (NEXAFS) spectroscopy is such a tool. It has been used for investigating the unoccupied orbitals of organometallic dye molecules,[12−21] as well as of complexes consisting of electron-donating groups.[22,23] Here we utilize this capability to distinguish N 1s-to-π* transitions of N atoms belonging to the donor and the light-harvester components of a D−π−A porphyrin-based sensitizer. Furthermore, orbitals characteristic of all three constituent groups—donor, π-bridge, acceptor—are identified by combining data from the C 1s and N 1s edges. This ability of NEXAFS to individually probe the contribution of each group facilitates the controlled design and optimization of DSSCs with "push−pull" architecture. To complement the element-specific NEXAFS results, we have also used ultraviolet/visible (UV/vis) spectroscopy to obtain the optical band gap and the position of the highest occupied molecular orbital (HOMO).

Two custom-synthesized organometallic molecules are investigated, named GT14[24] and GT15[24,25] (Chart 1). The molecules consist of a zinc(II) porphyrin ring as large π-conjugated, main absorbing unit, that is functionalized with a 4-ethynylbenzoic group at a meso-position as the electron-withdrawing and anchoring moiety. GT15 has a "push−pull" architecture with triphenylamine groups attached to the porphyrin ring. Amine moieties are known to be strong electron donors through resonance effects. GT14, on the other hand, holds isopropyl groups linked to the phenyl rings at meso-positions, which behave as weak donors through inductive effects. The position of the isopropyl groups in GT14 was chosen based on previous results with tetraphenylporphyrin sensitizers, which established that substitution with alkoxy-chains at the ortho-position of the meso-phenyl groups increases the efficiencies of the cells.[26] An additional molecule consisting exclusively of electron-donating amine groups [1,3,5-tris(diphenylamino)benzene, tris(DPA)] is also

investigated as a reference for the donor levels (see Chart 1). The electron-donating properties of nitrogen in amine groups originate from the atom's lone pair electrons. These are available to participate in resonance effects through π-bonds. Compared to the highly polar carboxylic moiety, amine groups are less electronegative (less acidic). Electron donation is thus a result of a gradient in electronegativity. This is different from the use of group-V elements as donors in σ-bonded group-IV semiconductors. There, the electron-donating properties of the dopant are due to its extra valence electron, which is injected into the conduction band of the semiconductor to increase the charge carrier density.

Theoretical understanding of the X-ray and optical absorption spectra of the investigated molecules is obtained via ab initio simulations using the eXcited electron and Core-Hole (XCH) approach[27] and time-dependent density functional theory (TDDFT),[28] respectively. The results demonstrate the influence of the electron-donating groups on the position of the band edges, as well as on the degree of localization of the frontier molecular orbitals. In particular, it is concluded that the attachment of electron-donating groups to the porphyrin ring leads to a significant delocalization of the HOMO, as well as to an increase of its energy, resulting in a decrease of the quasiparticle band gap by the same amount. The lowest unoccupied molecular orbital (LUMO), on the other hand, remains localized and does not significantly change its energy. These conclusions provide new insights into the factors which contribute to the high energy conversion efficiencies of D−π−A molecules.

■ EXPERIMENTAL AND THEORETICAL METHODS

The synthesis of the dye molecules has been described elsewhere.[24,25] Their chemical purity was verified with high-resolution mass spectroscopy (HRMS) characterization. The reference molecule tris(DPA) was obtained from Sigma-Aldrich.

NEXAFS spectroscopy was used to selectively probe the electronic states located at the N and C atoms via the N 1s and C 1s absorption edges. The NEXAFS work was conducted at

Beamline 8.0.1 of the Advanced Light Source (ALS) at Lawrence Berkeley National Laboratory. The details of the NEXAFS experiments, including photon energy calibration and normalization to the photon flux, have been described in previous publications.[21,29] All spectra presented in the following were measured by detecting the total electron yield (TEY). The data points were interpolated with a cubic spline function. The background from the tail of low-energy absorption edges was subtracted by a linear fit.

For the NEXAFS studies, 0.4 mmol solutions of the dye powders were prepared in anhydrous tetrahydrofuran (THF). The solutions were briefly placed in an ultrasound bath (for about 60 s) to ensure that the dyes were fully dissolved. The samples were prepared by drop-casting through glass pipets onto gold-coated silicon wafers. Fast drying of the samples, ensuring high homogeneity, was achieved with the help of a nitrogen stream flowing near the substrate surface inside a fume hood. The thickness of the samples was optimized to achieve the highest possible NEXAFS signal without significant sample charging occurring.

For the optical investigations, ultraviolet/visible spectroscopy was employed to study dilute solutions of GT14 and GT15 in chloroform ($CHCl_3$). A Hewlett-Packard 8453 spectrophotometer was used for these measurements. The spectra were referenced to pure chloroform.

Structural and electronic properties of GT14 and G15 molecules were investigated via ab initio ground-state density functional theory (DFT) total energy calculations,[30,31] as well as via K-edge X-ray and optical absorption spectroscopy simulations. Since X-ray absorption measurements were performed in high vacuum conditions, geometry optimizations for the purpose of NEXAFS simulations were carried out on isolated molecules in the gas phase, using the standard projector augmented wave DFT implementation within the VASP package.[32] A planewave cutoff of 350 eV was employed and atomic positions were optimized until all forces were smaller than 0.01 eV/Å. For the exchange-correlation (XC) functional, the generalized gradient approximation of Perdew, Burke, and Ernzerhof[33] (PBE) was employed. The electron−ion interaction was described by pseudopotentials featuring valence electronic configurations of Zn: [Ar] $4s^2$, $3d^{10}$; O: [He] $2s^2$, $2p^4$; N: [He] $2s^2$, $2p^3$; C: [He] $2s^2$, $2p^2$; H: $1s^1$. Predicted structures of the Zn-porphyrin molecules are in good agreement with experimental geometries,[34] with an average Zn−N distance within the porphyrin core of 2.045 Å (2.051 Å) in GT14 (GT15). Test calculations using the B3LYP XC functional (within a Gaussian basis-set framework described below) yield average Zn−N distances in the gas phase that are only 0.1% longer than the PBE estimates. NEXAFS simulations at the N K-edge were carried out using the XCH approach[27,35] implemented in an in-house development version of the Quantum-Espresso[36] suite of programs. Within this approach, pseudopotentials are employed to model core-excited atoms and excitation energies are estimated from ΔSCF total-energy differences.[37,38] Importantly, the full electronic core hole and the screening due to the excited electron are self-consistently taken into account. Technical details of the XCH method have been described in detail elsewhere.[27,35] Within Quantum-Espresso based simulations, a planewave cutoff of 25 Ry was used in conjunction with ultrasoft pseudopotentials,[39] having the same configuration as above.

Optical spectra were simulated using TDDFT[28] within the Tamm−Dancoff approximation[40] as implemented in the

GAMESS quantum chemistry package.[41] The NOSeC-V-DZP[42] contracted Gaussian-type function basis sets and associated model core potentials (MCPs) were employed for O, N, and C, while the NOSeC-V-TZP[43] basis set and corresponding MCP were employed for Zn. A Dunning triple-ζ valence basis set[44] was used for H. Since experimental UV/vis measurements were performed on dilute solutions of GT14 and GT15 in chloroform, molecular structures employed in the optical absorption simulations were separately optimized, including an implicit solvent within a conductor-like polarizable continuum model (CPCM).[45] Structural optimizations were performed at the B3LYP[43] level. The overall structure around the Zn site in the solvated case is found to be similar to that in the gas phase, with the average Zn−N bond length at 2.052 Å (2.058 Å) in GT14 (GT15). TDDFT excitation energies were calculated using both the B3LYP and the Coulomb attenuated CAM-B3LYP[46] exchange-correlation functionals. A uniform Gaussian broadening of 0.2 eV (0.05 eV) was applied to the calculated NEXAFS (optical) spectra.

■ RESULTS AND DISCUSSION

Ultraviolet/Visible Absorption Spectroscopy. Ultraviolet/visible absorption spectra of GT14 and GT15 solutions in chloroform ($CHCl_3$) are shown in Figure 1. The spectra exhibit strong Soret peaks corresponding to transitions to the second excited state (S0 → S2) at wavelengths 422 nm for GT14 (a) and 446 nm for GT15 (b). The molecules thus absorb strongly in the violet and blue regions of the solar spectrum. Weaker, Q-band peaks corresponding to transitions to the first excited state (S0 → S1) are observed at wavelengths
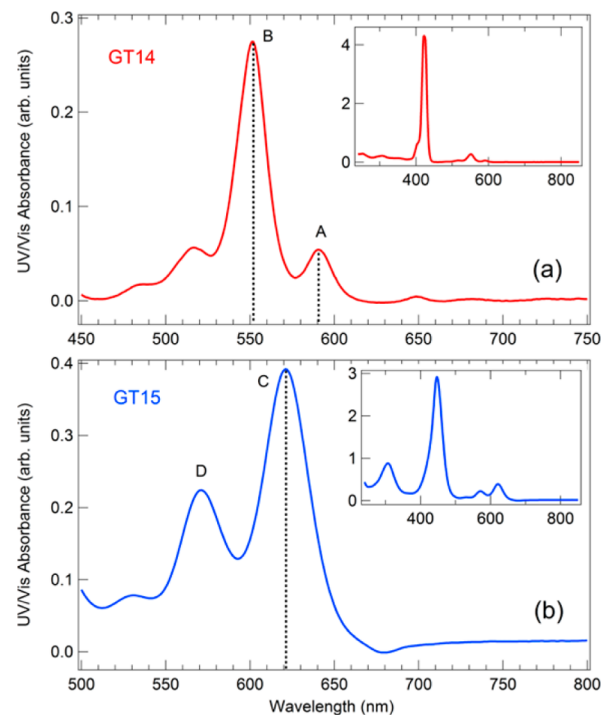
Figure 1. Ultraviolet/visible (UV/vis) absorption spectra of GT14 (a) and GT15 (b) solutions in chloroform ($CHCl_3$). The lowest energy peak is at 2.25 eV (551 nm) for GT14 (B) and at 2.00 eV (621 nm) for GT15 (C). The optical transition associated with peak A (591 nm) originates from partial demetalation of GT14. The inset shows an extended photon energy range, which includes the strong Soret peaks at wavelengths of 422 nm for GT14 and 446 nm for GT15.

between 517 and 591 nm for GT14, and between 571 and 621 nm for GT15. Both Soret and Q bands arise from $\pi-\pi^*$ transitions and can be explained based on the Gouterman four-orbital model.[47−49] In GT15, the transitions are broader and shifted toward larger wavelengths compared to GT14. The weak peak at the low-energy (high-wavelength) end of the Q-band corresponds to the lowest excitonic transition for each dye. It occurs at 2.25 eV (551 nm) for GT14 (peak B) and at 2.00 eV (621 nm) for GT15 (peak C). Peak A at 2.10 eV (591 nm) in the GT14 spectrum originates from partial demetalation of the molecule, as will be explained in the following. These energies represent lower-limits for the HOMO−LUMO gaps of these molecules. Accordingly, the HOMO−LUMO gap in GT15 is 0.25 eV smaller than that in GT14. This is favorable for solar light absorption, as it brings the gap closer to the optimum for a single-junction cell (about 1.1−1.4 eV).

X-ray Absorption Spectroscopy. Figure 2 shows X-ray absorption spectra at the N 1s edge of GT14 and GT15. A
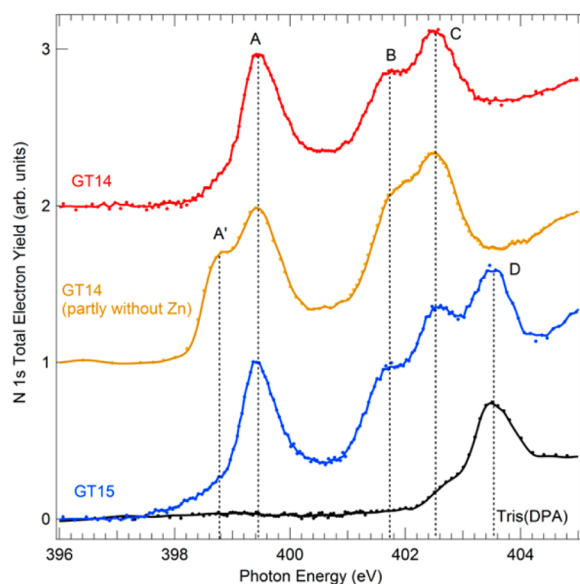
Figure 2. N 1s absorption spectra of GT14 and GT15, drop-cast from solutions in THF. A reference spectrum of tris(DPA) is also shown for comparison. Peaks A, B, and C all originate from the pyrrole subunits of the central porphyrin ring. Peak D appears only in GT15. Based on the comparison with the tris(DPA) spectrum, it is assigned to the electron-donating triphenylamine groups. Feature A′ appears as a result of symmetry lowering in demetalated GT14 molecules.

reference spectrum of tris(diphenylamino)benzene (tris(DPA)) is also shown for comparison. The spectra of both porphyrins exhibit three peaks at photon energies 399.4 eV (A), 401.7 eV (B), and 402.5 eV (C), which are all attributed to the nitrogen atoms of the porphyrin ring. A fourth peak (D) is present at energy 403.5 eV in GT15, while it is completely absent in GT14. Upon comparison with the reference tris(DPA) spectrum, which exhibits a peak at the same energy position, it becomes obvious that this feature originates from the nitrogen atoms of the electron-donating triphenylamine groups which are attached to the porphyrin ring in GT15.

A prolonged stay of GT14 in solution can lead to partial demetalation of the molecule, namely removal of the central Zn atom of the porphyrin ring. Previous studies have shown that the inverse process, i.e., a transfer of a Zn atom to the center of a Zn-free protoporphyrin adsorbed on a ZnO substrate, can

easily occur.[29] After the demetalation, two of the N atoms of the pyrrol subunits are connected to H atoms, while the other two N atoms possess lone pair electrons and do not form new bonds. The result is the appearance of a low-energy shoulder (A′) in the N 1s absorption spectrum of GT14, approximately 0.6 eV below peak A (Figure 2). Feature A′ is attributed to the N 1s → π^* transitions of the lone-pair N atoms of the ring. This was confirmed by ab initio calculations, as will be explained in the following. GT15 is less prone to demetalation, possibly because its triphenylamine groups distort to a smaller extent the planarity of the porphyrin ring compared to the isopropyl groups in GT14.

Figure 3 shows C 1s absorption spectra of the two dye molecules, compared to the reference molecule tris(DPA). The
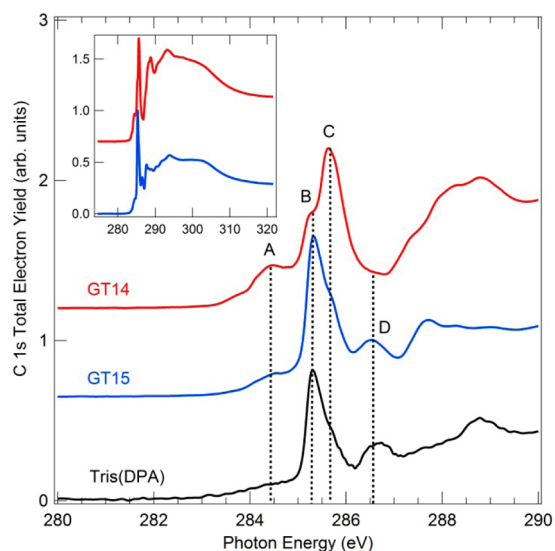
Figure 3. Comparison of C 1s TEY absorption spectra of GT14 and GT15, drop-cast from solutions in THF. The main plot focuses on the π^* region of the spectra, while the inset shows the entire energy range, including the σ^* features. Upon comparison with the reference absorption spectrum of tris(DPA), it is concluded that peaks A (284.5 eV) and C (285.6 eV) originate mainly from C 1s → π^* transitions in the central porphyrin ring. Peak B (285.3 eV) has its strongest contribution from the electron-donating triphenylamine groups, and peak D (286.5 eV) is exclusively due to the electron donors.

spectra of the two dyes exhibit a dominant double peak with maxima at 285.3 eV (B) and 285.6 eV (C). Peak B, which is also present in the spectrum of tris(DPA), has higher intensity in GT15. A weaker, low-energy feature is present at 284.5 eV (A) in both dyes. GT15 exhibits an additional feature at 286.5 eV (D). This feature is observed in tris(DPA) as well, while it is completely absent in GT14. On the basis of these observations, we conclude that peaks A and C predominantly originate from C 1s → π^* transitions in the porphyrin bridge, with carbon–carbon (C=C) double bonds in the pyrrole subunits being the strongest contribution, in accordance with previous reports.[50,51] Peak B has its highest contribution from the peripheral electron-donating triphenylamine groups and a smaller contribution from the porphyrin ring, thus having higher intensity in GT15. Peak D is exclusively due to the carbon atoms of the electron donors and is only present in the molecules which contain amine groups. The broad features above 287 eV correspond to C 1s → σ^* transitions originating from C atoms in carbon–carbon and carbon–oxygen σ-bonds.

These assignments are consistent with DFT calculations performed at the C 1s edge (not shown). Although the calculations cannot distinguish between peaks B and C, they do reproduce all main features of the experimental NEXAFS spectra of Figure 3, including the smaller intensity of feature A in GT15 compared to GT14, the absence of feature A from tris(DPA), and the stronger σ^* features in GT14 compared to GT15.

DFT and TDDFT Calculations. In order to identify the nature of the frontier orbitals in GT14 and GT15, we performed both ground-state DFT calculations and NEXAFS simulations using the eXcited electron and Core Hole approach (XCH) at the N 1s edge. The calculated spectra are in good agreement with the experimental NEXAFS results (see Figure 4a). All major features of the X-ray absorption spectra are well reproduced, including the number of the observed peaks, their
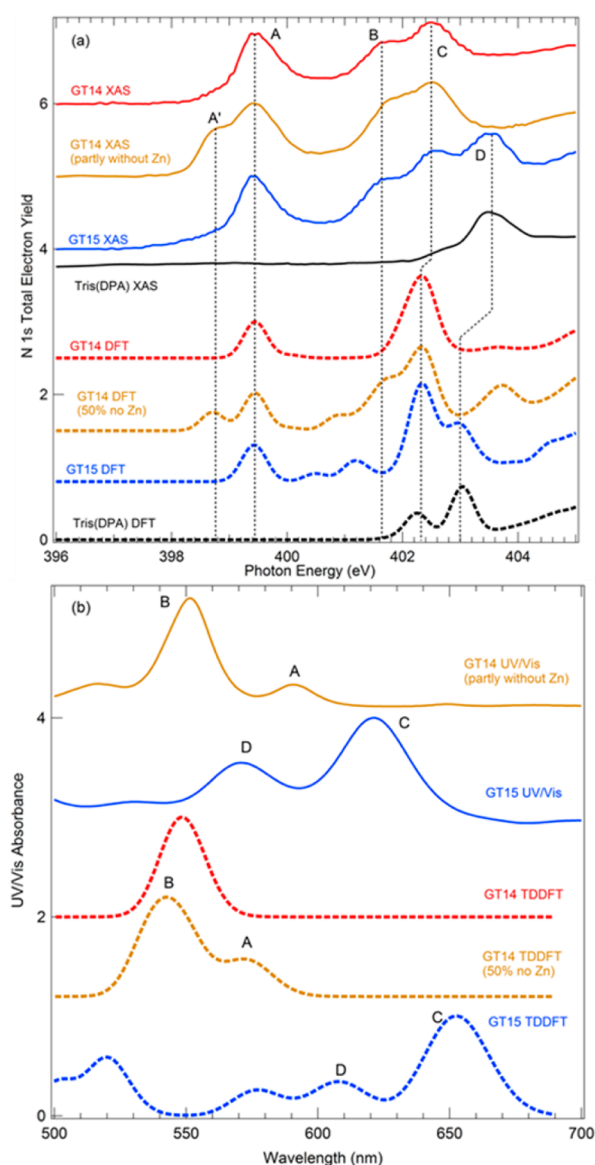
Figure 4. Theoretical DFT (a) and TDDFT (b) spectra (dashed lines), compared with the experimental NEXAFS (a) and ultraviolet/visible (b) spectra (solid lines) of GT14 and GT15. The theoretical and experimental NEXAFS spectra of the reference molecule tris(DPA) are also shown for comparison.

relative energy positions and even their relative intensities. The appearance of the low-energy feature A′ can be reproduced by assuming a lowering of the molecular symmetry as a result of partial demetalation of the porphyrin ring. In the demetalated molecule, two of the four N sites in the porphyrin core are protonated, while the other two remain nonpassivated and host lone pairs. These lone pairs interact only weakly with the H atoms bonded to the two other N sites. The higher local charge density on the lone-pair N sites results in a shallower 1s core-level and a smaller 1s → π^* excitation energy corresponding to the feature A′. The fact that peak B is present in the experimental spectrum of GT14, while it is absent in the simulation of the nondemetalated molecule, may indicate either that some degree of demetalation was present even in the nominally nondemetalated molecule, or that some other symmetry-lowering mechanism, which was not accounted for in the calculations, is present. We note that the inclusion of vibrational effects in the NEXAFS simulations (by averaging the spectra over a 300 K molecular dynamics trajectory of the nondemetalated molecules) only leads to a slight broadening of the spectral features, without giving rise to feature B.

Interestingly, the energy of the first 1s → π^* transition is practically identical in the two molecules. This is indicated by the position of peak A in the N 1s spectra: it remains unchanged upon attachment of the donor group, both in the NEXAFS results and in the theoretical simulations. This suggests that the nature of the LUMO and the associated final state in the core-excited configuration is rather similar in GT14 and GT15.

Ground-state DFT calculations using the B3LYP XC functional indicate that the spatial extent of the LUMO is similar in GT14 and GT15, with no significant change upon attachment of the electron-donating functional groups. In both molecules, it extends primarily to the N atoms of the porphyrin ring and the C atoms of the carboxylic and benzene moieties of the acceptor group. This is in agreement with previous knowledge that the LUMO in Zn porphyrins is a π^*-orbital located primarily in the porphyrin core.[13,14,51] However, the nature of the HOMO is significantly different in the two molecules: while in GT14, it is localized in the porphyrin ring, in GT15 it is completely delocalized, distributed over the N atoms of the triphenylamine donor groups, the central Zn atom and the C and N atoms of the porphyrin ring. A three-dimensional representation of the frontier orbitals in the two molecules is shown in Figure 5. The main conclusion from the above results is that, while the HOMO and LUMO in GT14 are located in the same part of the molecule, namely the porphyrin ring and to a smaller extent the acceptor group, in GT15 there is a significant spatial separation of the two: the LUMO is partly located in the acceptor group, while the HOMO in the donor group, with some overlapping only within the porphyrin ring. The same is found for the orbitals HOMO-1 and LUMO+1 (Figure S1 of the Supporting Information, SI): they are both located in the porphyrin ring in GT14, while they do not overlap at all in GT15. This situation results in better spatial separation of light-induced electrons and holes in GT15 upon solar illumination, which reduces the recombination rate, thus enhancing the output current. Related conclusions have been previously reached in theoretical studies discussing the spatial separation of the frontier orbitals in polypyridine[53,54]- and phthalocyanine-based[55] molecular structures.

HOMO and LUMO quasiparticle (QP) energies, corresponding to the ionization potential (IP) and electron affinity
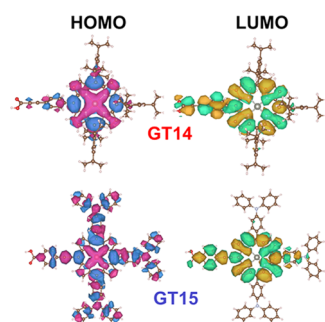
Figure 5. Three-dimensional representations of the frontier orbitals (HOMO, LUMO) of GT14 and GT15 based on ground-state DFT calculations. The HOMO of GT15 is delocalized, extending to the N atoms of the electron-donating groups, while the LUMO remains localized in the porphyrin ring and the acceptor group. This results in spatial separation of the light-induced electrons and holes.

(EA), were calculated from B3LYP total-energy differences using a ΔSCF approach. The results are shown in Table 1. The

Table 1. Calculated Quasiparticle (QP) Energies of Frontier Orbitals (IP: Ionization Potential; EA: Electron Affinity), and the Associated QP Gap (from Ground-State DFT) and Optical Gap (from TDDFT), for Both the Gas Phase and the Solvated Phase of the Molecules

	gas phase			in solution (CHCl$_3$ solvent)			
	IP (eV)	EA (eV)	QP gap (eV)	IP (eV)	EA (eV)	QP gap (eV)	optical gap (eV)
GT15	5.53	1.84	3.69	4.84	2.61	2.23	1.90
GT14	6.07	1.62	4.45	5.13	2.34	2.79	2.26
GT14 (no Zn)	5.99	1.67	4.32	5.19	2.44	2.75	2.16

QP gap in the gas phase is 0.76 eV larger in GT14 than in the D−π−A molecule GT15. The main contribution to this difference is from the HOMO levels, while the LUMO energies are much closer. This is consistent with previous DFT studies on substituted Zn porphyrins, which found that the variation of electron donors attached to the porphyrin ring mainly affects the HOMO energy level.[56]

Optical spectra calculated from TDDFT at the B3LYP level are shown in Figure 4b and compared to the experimental UV/vis spectra. The calculations indicate that the optical gap is 0.36 eV smaller in GT15 than in GT14 in the PCM solvated phase (Table 1, last column). This is in good agreement with the

experiment. The agreement between calculations and experiment is further improved under the assumption of partial demetalation of GT14. The theoretical optical absorption spectrum of GT14 contains one single peak roughly at the position of experimental peak B, while the higher-wavelength peak A appears in the calculations only for the partly demetalated molecule. This means that partial demetalation of GT14 is unavoidable, or at least very likely, when the molecule is dissolved (as required for the UV/vis measurements).

In order to be able to compare the TDDFT-calculated optical gap with the QP gap from ground-state DFT, we calculated the QP gap also for the solvated phase (Table 1). As expected, the QP gap is in both molecules larger than the energy of the lowest optical transition because of the exciton binding energy. For the lowest singlet excitation, we estimate the exciton binding energy to be equal to 0.33 eV in GT15 and 0.53 eV in GT14. The higher binding energy in GT14 can be explained based on the larger spatial overlap between the HOMO and LUMO wave functions in GT14, as discussed earlier, which leads to a stronger electron−hole interaction. It is noted that in the PCM solvated case, the calculated QP gaps are smaller than in the gas phase. The difference in the QP gap between GT14 and GT15 is also smaller (0.56 eV vs 0.76 eV in the gas phase).

For both molecules, B3LYP spectra are in better agreement than CAM-B3LYP (not shown) as far as the low-energy (high wavelength) excitations are concerned (in the yellow-green region of the spectrum). The orbital overlap quantity Λ, which is known to be correlated to the B3LYP excitation energy errors, has a value higher than 0.6, indicating reliable functional performance[52] (see Table 2). Although for higher-energy excitations (in the blue-violet region), B3LYP tends to overestimate the charge-transfer character and underestimate the energy position of the excitations (Table S1 of the SI), it is clearly the better choice in this case for simulating the optical spectra around the excitations which are relevant for determining the HOMO−LUMO optical gap.

The different spatial extent of the HOMO in the two molecules, which was concluded based on the ground-state DFT calculations, is also reflected in the TDDFT calculations of the optical spectra, both when B3LYP and when CAM-B3LYP is used as the XC functional. The lowest energy singlet excitation, which is primarily composed of a HOMO to LUMO transition, has a lower Λ parameter value in GT15 (Table 2). This is indicative of a more charge-transfer-like nature of the HOMO−LUMO excitation in GT15 and a more localized

Table 2. Character of the Lowest Energy Singlet Excitation in GT15 and GT14, as Obtained from TDDFT Calculations, both for B3LYP and for CAM-B3LYP Functionals[a]

	functional	energy (eV)	oscillator strength	primary character (occupied → virtual)			Λ parameter
				occupied orbital	virtual orbital	weight (%)	
GT15	B3LYP	1.90	0.667	HOMO	LUMO	88.5	0.634
				HOMO−4	LUMO+1	9.8	
	CAM-B3LYP	2.14	0.497	HOMO	LUMO	68.5	0.692
				HOMO−1	LUMO+1	23.1	
GT14	B3LYP	2.260	0.070	HOMO	LUMO	61.0	0.731
				HOMO−1	LUMO+1	37.4	
	CAM-B3LYP	2.326	0.023	HOMO	LUMO	53.3	0.75
				HOMO−1	LUMO+1	42.9	

[a]The smaller Λ value of the HOMO−LUMO excitation in GT15 indicates less localized frontier orbitals than in GT14.

nature in GT14. The same trend is also observed for higher lying excitations in the visible range (Table S1 of the SI).

CONCLUSIONS

The electronic structure of custom porphyrin-based dye molecules with "donor−π−acceptor" structure was investigated with X-ray absorption spectroscopy, combined with optical absorption and ab initio calculations. The energies of the unoccupied orbitals, including the LUMO, as well as the position of the HOMO and the optical band gap were determined. The bond selectivity of X-ray absorption spectroscopy made it possible to identify molecular orbitals characteristic of each of the constituents—donor, π-bridge, and acceptor. A decrease of the optical band gap of the sensitizer by about 0.3 eV was found upon attachment of the electron-donating amine groups. This is favorable for efficient solar light absorption, as it brings the gap closer to the optimum for a single-junction cell. This decrease is attributed to a lowering of the ionization potential and a proportionate increase in the electron affinity. Furthermore, the attachment of electron-donating groups to the porphyrin ring results in significant delocalization of the HOMO, and thus in spatial separation between the HOMO and the LUMO. This reduces the recombination rate of light-induced electrons and holes within the molecule, thus increasing the energy-conversion efficiency. Such spectroscopic investigations of organometallic sensitizers with "push−pull" architecture are helpful for systematically increasing the efficiency of DSSCs by optimizing individual groups in donor−π-bridge−acceptor complexes.

ASSOCIATED CONTENT

Ⓢ Supporting Information

Figure S1 shows three-dimensional representations of the orbitals HOMO-1 and LUMO+1 in GT14 and GT15, based on ground-state DFT calculations. Table S1 shows calculated excitation energies, oscillator strengths, and Λ parameters for the five lowest energy singlet transitions in GT14 and GT15, obtained with TDDFT, using both B3LYP and CAM-B3LYP functionals. This material is available free of charge via the Internet at http://pubs.acs.org.

AUTHOR INFORMATION

Corresponding Author
*Tel.: 608-263-5590; fax: 608-265-2334; e-mail: fhimpsel@wisc.edu.

Notes
The authors declare no competing financial interest.

ACKNOWLEDGMENTS

REFERENCES

(1) O'Regan, B.; Grätzel, M. A Low-Cost, High-Efficiency Solar Cell Based on Dye-Sensitized Colloidal TiO$_2$ Films. *Nature* **1991**, *353*, 737−740.

(2) Chiba, Y.; Islam, A.; Watanabe, Y.; Komiya, R.; Koide, N.; Han, L. Dye-Sensitized Solar Cells with Conversion Efficiency of 11.1%. *Jpn. J. Appl. Phys.* **2006**, *45*, L638−L640.

(3) Hardin, B. E.; Snaith, H. J.; McGehee, M. D. The Renaissance of Dye-Sensitized Solar Cells. *Nat. Photonics* **2012**, *6*, 162−169.

(4) Yella, A.; Lee, H.-W.; Tsao, H. N.; Yi, C.; Chandiran, A. K.; Nazeeruddin, M. K.; Diau, E. W.-G.; Yeh, C.-Y.; Zakeeruddin, S. M.; Grätzel, M. Porphyrin-Sensitized Solar Cells with Cobalt (II/III)-Based Redox Electrolyte Exceed 12% Efficiency. *Science* **2011**, *334*, 629−634.

(5) Nazeeruddin, M. K.; De Angelis, F.; Fantacci, S.; Selloni, A.; Viscardi, G.; Liska, P.; Ito, S.; Takeru, B.; Grätzel, M. Combined Experimental and DFT-TDDFT Computational Study of Photoelectrochemical Cell Ruthenium Sensitizers. *J. Am. Chem. Soc.* **2005**, *127*, 16835−16847.

(6) Bessho, T.; Zakeeruddin, S. M.; Yeh, C.-Y.; Diau, E. W.-G.; Grätzel, M. Highly Efficient Mesoscopic Dye-Sensitized Solar Cells Based on Donor-Acceptor-Substituted Porphyrins. *Angew. Chem.* **2010**, *122*, 6796−6799.

(7) Wu, S.-L.; Lu, H.-P.; Yu, H.-T.; Chuang, S.-H.; Chiu, C.-L.; Lee, C.-W.; Diau, E. W.-G.; Yeh, C.-Y. Design and Characterization of Porphyrin Sensitizers with a Push-Pull Framework for Highly Efficient Dye-Sensitized Solar Cells. *Energy Environ. Sci.* **2010**, *3*, 949−955.

(8) Cai, N.; Moon, S.-J.; Cevey-Ha, L.; Moehl, T.; Humphry-Baker, R.; Wang, P.; Zakeeruddin, S. M.; Grätzel, M. An Organic D-π-A Dye for Record Efficiency Solid-State Sensitized Heterojunction Solar Cells. *Nano Lett.* **2011**, *11*, 1452−1456.

(9) Bai, Y.; Yu, Q.; Cai, N.; Wang, Y.; Zhang, M.; Wang, P. High-Efficiency Organic Dye-Sensitized Mesoscopic Solar Cells with a Copper Redox Shuttle. *Chem. Commun.* **2011**, *47*, 4376−4378.

(10) Zhang, X. L.; Huang, F.; Nattestad, A.; Wang, K.; Fu, D.; Mishra, A.; Bäuerle, P.; Bach, U.; Cheng, Y.-B. Enhanced Open-Circuit Voltage of p-Type DSC with Highly Crystalline NiO Nanoparticles. *Chem. Commun.* **2011**, *47*, 4808−4810.

(11) Martínez-Díaz, M. V.; De la Torre, G.; Torres, T. Lighting Porphyrins and Phthalocyanines for Molecular Photovoltaics. *Chem. Commun.* **2010**, *46*, 7090−7108.

(12) Cook, P. L.; Liu, X.; Yang, W.; Himpsel, F. J. X-ray Absorption Spectroscopy of Biomimetic Dye Molecules for Solar Cells. *J. Chem. Phys.* **2009**, *131*, 194701-1−194701-10.

(13) Cook, P. L.; Yang, W.; Liu, X.; García-Lastra, J. M.; Rubio, A.; Himpsel, F. J. Unoccupied States in Cu and Zn Octaethyl-Porphyrin and Phthalocyanine. *J. Chem. Phys.* **2011**, *134*, 204707−1−204707−7.

(14) García-Lastra, J. M.; Cook, P. L.; Himpsel, F. J.; Rubio, A. Communication: Systematic Shifts of the Lowest Unoccupied Molecular Orbital Peak in X-Ray Absorption for a Series of 3d Metal Porphyrins. *J. Chem. Phys.* **2010**, *133*, 151103−1−151103−4.

(15) Narioka, S.; Ishii, H.; Ouchi, Y.; Yokoyama, T.; Ohta, T.; Seki, K. XANES Spectroscopic Studies of Evaporated Porphyrin Films: Molecular Orientation and Electronic Structure. *J. Phys. Chem.* **1995**, *99*, 1332−1337.

(16) Polzonetti, G.; Carravetta, V.; Iucci, G.; Ferri, A.; Paolucci, G.; Goldoni, A.; Parent, P.; Laffon, C.; Russo, M. V. Electronic Structure of Platinum Complex/Zn-Porphyrinato Assembled Macrosystems, Related Precursors and Model Molecules, as Probed by X-Ray Absorption Spectroscopy (NEXAFS): Theory and Experiment. *Chem. Phys.* **2004**, *296*, 87−100.

(17) Rienzo, A.; Mayor, L. C.; Magnano, G.; Satterley, C. J.; Ataman, E.; Schnadt, J.; Schulte, K.; O'Shea, J. N. X-ray Absorption and Photoemission Spectroscopy of Zinc Protoporphyrin Adsorbed on Rutile TiO$_2$(110) Prepared by In Situ Electrospray Deposition. *J. Chem. Phys.* **2010**, *132*, 084703−1−084703−6.

(18) Cudia, C. C.; Vilmercati, P.; Larciprete, R.; Cepek, C.; Zampieri, G.; Sangaletti, L.; Pagliara, S.; Verdini, A.; Cossaro, A.; Floreano, L.; et al. Electronic Structure and Molecular Orientation of a Zn-tetraphenyl Porphyrin Multilayer on Si(111). *Surf. Sci.* **2006**, *600*, 4013−4017.

(19) Campbell, W. M.; Burrell, A. K.; Officer, D. L.; Jolley, K. W. Porphyrins as Light Harvesters in the Dye-Sensitised TiO$_2$ Solar Cell. *Coord. Chem. Rev.* **2004**, *248*, 1363−1379.

(20) Rangan, S.; Katalinic, S.; Thorpe, R.; Bartynski, R. A.; Rochford, J.; Galoppini, E. Energy Level Alignment of a Zinc (II) Tetraphenylporphyrin Dye Adsorbed onto TiO$_2$(110) and ZnO(11−20) Surfaces. *J. Phys. Chem. C* **2010**, *114*, 1139−1147.

(21) Zegkinoglou, I.; Cook, P. L.; Johnson, P. S.; Yang, W.; Guo, J.; Rogero, C.; Ruther, R. E.; Rigsby, M. L.; Ortega, E.; Hamers, R. J.; et al. Electronic Structure of Diamond Surfaces Functionalized by Ru(tpy)2. *J. Phys. Chem. C* **2012**, *116*, 13877−13883.

(22) Ade, H.; Hitchcock, A. P. NEXAFS Microscopy and Resonant Scattering: Composition and Orientation Probed in Real and Reciprocal Space. *Polymer* **2008**, *49*, 643−675.

(23) Watts, B.; Swaraj, S.; Nordlund, D.; Lüning, J.; Ade, H. Calibrated NEXAFS Spectra of Common Conjugated Polymers. *J. Chem. Phys.* **2011**, *134*, 024702−1−024702−15.

(24) Ragoussi, M. E.; de la Torre, G.; Torres, T. Tuning the Electronic Properties of Porphyrin Dyes: Effects of meso-Substitution on their Optical and Electrochemical Behaviour. *Eur. J. Org. Chem.* **2013**, 2832−2840.

(25) Liu, B.; Zhu, W.; Wang, Y.; Wu, W.; Li, X.; Chen, B.; Long, Y.-T.; Xie, Y. Modulation of Energy Levels by Donor Groups: An Effective Approach for Optimizing the Efficiency of Zinc-Porphyrin Based Solar Cells. *J. Mater. Chem.* **2012**, *22*, 7434−7444.

(26) Wang, C.-L.; Lan, C.-M.; Hong, S.-H.; Wang, Y.-F.; Pan, T.-Y.; Chang, C.-W.; Kuo, H.-H.; Kuo, M.-Y.; Diau, E. W.-G.; Lin, C.-Y. Enveloping Porphyrins for Efficient Dye-Sensitized Solar Cells. *Energy Environ. Sci.* **2012**, *5*, 6933−6940.

(27) Prendergast, D.; Galli, G. X-Ray Absorption Spectra of Water from First Principles Calculations. *Phys. Rev. Lett.* **2006**, *96*, 215502−1−215502−4.

(28) Runge, E.; Gross, E. K. U. Density-Functional Theory for Time-Dependent Systems. *Phys. Rev. Lett.* **1984**, *52*, 997−1000.

(29) González-Moreno, R.; Cook, P. L.; Zegkinoglou, I.; Liu, X.; Johnson, P. S.; Yang, W.; Ruther, R. E.; Hamers, R. J.; Tena-Zaera, R.; Himpsel, F. J.; et al. Attachment of Protoporphyrin Dyes to Nanostructured ZnO Surfaces: Characterization by Near Edge X-ray Absorption Fine Structure Spectroscopy. *J. Phys. Chem. C* **2011**, *115*, 18195−18201.

(30) Hohenberg, P.; Kohn, W. Inhomogeneous Electron Gas. *Phys. Rev.* **1964**, *136*, B864−B871.

(31) Kohn, W.; Sham, L. J. Self-Consistent Equations Including Exchange and Correlation Effects. *Phys. Rev.* **1965**, *140*, A1133−A1138.

(32) Kresse, G.; Furthmüller, J. Efficient Iterative Schemes for Ab Initio Total-Energy Calculations Using a Plane-Wave Basis Set. *Phys. Rev. B* **1996**, *54*, 11169−11186.

(33) Perdew, J. P.; Burke, K.; Ernzerhof, M. Generalized Gradient Approximation Made Simple. *Phys. Rev. Lett.* **1996**, *77*, 3865−3868.

(34) Fleischer, E. B. The Structure of Porhyrins and Metalloporphyrins. *Acc. Chem. Res.* **1970**, *3*, 105−112.

(35) England, A. H.; Duffin, A. M.; Schwartz, C. P.; Uejio, J. S.; Prendergast, D.; Saykally, R. J. On the Hydration and Hydrolysis of Carbon Dioxide. *Chem. Phys. Lett.* **2011**, *514*, 187−195.

(36) Giannozzi, P.; Baroni, S.; Bonini, N.; Calandra, M.; Car, R.; Cavazzoni, C.; Ceresoli, D.; Chiarotti, G. L.; Cococcioni, M.; Dabo, I.; et al. QUANTUM ESPRESSO: A Modular and Open-Source Software

Project for Quantum Simulations of Materials. *J. Phys.: Condens. Matter* **2009**, *21*, 395502−1−395502−19.

(37) Hedin, L.; Johansson, A. Polarization Corrections to Core Levels. *J. Phys. B* **1969**, *2*, 1336−1346.

(38) Kolczewski, C.; Püttner, R.; Plashkevych, O.; Ågren, H.; Staemmler, V.; Martins, M.; Snell, G.; Schlachter, A. S.; Sant'Anna, M.; Kaindl, G.; et al. Detailed Study of Pyridine at the C 1s and N 1s Ionization Thresholds: The Influence of the Vibrational Fine Structure. *J. Chem. Phys.* **2001**, *115*, 6426−6437.

(39) Vanderbilt, D. Soft Self-Consistent Pseudopotentials in a Generalized Eignevalue Formalism. *Phys. Rev. B* **1990**, *41*, 7892−7895.

(40) Hirata, S.; Head-Gordon, M. Time-Dependent Density Functional Theory within the Tamm−Dancoff Approximation. *Chem. Phys. Lett.* **1999**, *314*, 291−299.

(41) Schmidt, M. W.; Baldridge, K. K.; Boatz, J. A.; Elbert, S. T.; Gordon, M. S.; Jensen, J. H.; Koseki, S.; Matsunaga, N.; Nguyen, K. A.; Shujun, S.; et al. General Atomic and Molecular Electronic Structure System. *J. Comput. Chem.* **1993**, *14*, 1347−1363.

(42) Sakai, Y.; Miyoshi, E.; Klobukowski, M.; Huzinaga, S. Model Potentials for Main Group Elements Li through Rn. *J. Chem. Phys.* **1997**, *106*, 8084−8092.

(43) Osanai, Y.; Mon, M. S.; Noro, T.; Mori, H.; Nakashima, H.; Klobukowski, M.; Miyoshi, E. Revised Model Core Potentials for First-Row Transition-Metal Atoms from Sc to Zn. *Chem. Phys. Lett.* **2008**, *452*, 210−214.

(44) Dunning, T. H. Gaussian Basis Functions for Use in Molecular Calculations. III. Contraction of (10s6p) Atomic Basis Sets for the First-Row Atoms. *J. Chem. Phys.* **1971**, *55*, 716−723.

(45) Li, H. Quantum Mechanical/Molecular Mechanical/Continuum Style Solvation Model: Linear Response Theory, Variational Treatment, and Nuclear Gradients. *J. Chem. Phys.* **2009**, *131*, 184103−1−184103−8.

(46) Yanai, T.; Tew, D. P.; Handy, N. C. A New Hybrid Exchange−Correlation Functional Using the Coulomb-Attenuating Method (CAM-B3LYP). *Chem. Phys. Lett.* **2004**, *393*, 51−57.

(47) Gouterman, M. Study of the Effects of Substitution on the Absorption Spectra of Porphin. *J. Chem. Phys.* **1959**, *30*, 1139−1161.

(48) Gouterman, M. Spectra of Porphyrins. *J. Mol. Spectrosc.* **1961**, *6*, 138−163.

(49) Baerends, E.; Ricciardi, G. A DFT/TDDFT Interpretation of the Ground and Excited States of Porphyrin and Porphyrazine Complexes. *Coord. Chem. Rev.* **2002**, *230*, 5−7.

(50) Sivkov, V. N.; Zabrodina, G. S.; Nekipelov, S. V.; Petrova, O. V.; Shchupak, E. A.; Vyalikh, D. V.; Molodtsov, S. L. NEXAFS Study of Zinc Porphyrins Intercalated into V$_2$O$_5$ Xerogel. *Macroheterocycles* **2011**, *4*, 213−215.

(51) Schmidt, N.; Fink, R.; Hieringer, W. Assignment of Near-Edge X-Ray Absorption Fine Structure Spectra of Metalloporphyrins by Means of Time-Dependent Density-Functional Calculations. *J. Chem. Phys.* **2010**, *133*, 054703-1−054703-13.

(52) Peach, M. J. G.; Benfield, P.; Helgaker, T.; Tozer, D. J. Excitation Energies in Density Functional Theory: an Evaluation and a Diagnostic Test. *J. Chem. Phys.* **2008**, *128*, 044118-1−044118-8.

(53) Schott, E.; Zarate, X.; Arratia-Perez, R. Substituent Effects on Two Related Families of Dyes for Dye Sensitized Solar Cells: [Ru(4,4′-R,R-2,2′-bpy)$_3$]$^{2+}$ and [Ru(4,4′-COOH-2,2′-bpy)(4,4′-R,R-2,2′-bpy)$_2$]$^{2+}$. *J. Phys. Chem. A* **2012**, *116*, 7436−7442.

(54) Lachaud, F.; Jeandon, C.; Monari, A.; Assfeld, X.; Beley, M.; Ruppert, R.; Gros, P. C. Molecular Design of Porphyrins for Dye-Sensitized Solar Cells: A DFT/TDDFT Study. *Dalton Trans.* **2012**, *41*, 12865−12871.

(55) Zarate, X.; Schott, E.; Gomez, T.; Arratia-Pérez, R. Theoretical Study of Sensitizer Candidates for Dye-Sensitized Solar Cells: Peripheral Substituted Dizinc Pyrazinoporphyrazine-Phthalocyanine Complexes. *J. Phys. Chem. A* **2013**, *117*, 430−438.

(56) Santhanamoorthi, N.; Lo, C.-M.; Jiang, J.-C. Molecular Design of Porphyrins for Dye-Sensitized Solar Cells: A DFT/TDDFT Study. *J. Phys. Chem. Lett.* **2013**, *4*, 524−530.